Microchemical Journal 224 (2026) 117905



Contents lists available at ScienceDirect

Microchemical Journal

journal homepage: www.elsevier.com/locate/microc



Integrated non-invasive analysis of ceramic test sherds from the Iznik tile kilns excavation

Vesile Belgin Demirsar Arli [a,b], Gulsu Simsek-Franci [b,c,*]

[a] Istanbul University, Faculty of Letters, Department of Art History, Balabanaga Mah. Ordu Cad. No: 6 Laleli, Fatih, 34134 Istanbul, Türkiye
[b] Directorate of Iznik Tile Kilns Excavation, Yeşil Cami Mahallesi, Sultan Orhan Caddesi, 103/1 Iznik, 16860 Bursa, Türkiye
[c] Yildiz Technical University, Department of Metallurgical and Materials Engineering, Davutpasa Campus, 34220 Esenler Istanbul, Türkiye

ARTICLE INFO

Keywords:
pXRF
Raman
Experimental
Glaze
Iznik
Stonepaste
Paint

ABSTRACT

Since 2010, almost every excavation season at the Iznik Tile Kilns has yielded ceramic- and tile-type samples interpreted as experimental trials carried out by ceramicists prior to the main production of the splendid Iznik masterpieces. These samples show that primary decorative colors and their tonal variations were applied using brushes of varying thicknesses, different transparent glaze compositions were tested, and holes were intentionally made, likely to evaluate glaze viscosity during firing. In this study, the analytical results obtained from 20 ceramic-type test sherds with minimal surface deterioration are presented using non-invasive analytical techniques, including digital microscopy, portable XRF, and confocal Raman spectroscopy. Both sides of the samples are decorated and glazed. Microscopic examination revealed that the glaze thickness varies between approximately 100 and 420 μm, while the slip thickness ranges between 150 and 850 μm. The body colors vary from white to dark beige, whereas the slips appear either quartz-rich white or clay-rich beige in tone. Except for one sample, all specimens contain a lead–alkali transparent glaze (22–40 wt% PbO). The amount of tin oxide in the glazes was found to be below 1%. Body composition analyses indicate that all samples, except one, were produced according to a stonepaste recipe, while one sample appears relatively richer in clay compared to the stonepaste group. Overall, these results suggest that the analyzed sherds represent experimental productions from Iznik workshops, likely dating to the 17th century, aimed at exploring variations in color hues and glaze compositions prior to standardized manufacture.

1. Introduction

The Iznik Tile Kilns Excavation (İÇFK) represents one of the most significant archaeological projects in Türkiye, having revealed workshops and kilns associated with both Byzantine (14th century and earlier) and Ottoman (14th–17th centuries) ceramic and tile production in Iznik (formerly Nicaea during the Byzantine Empire, shown on the map of Anatolia [1] in the 14th century, see Fig. S1a). Research on Iznik ceramics and tiles was first initiated by Istanbul University in 1963. Although interrupted in 1969, excavations resumed in 1981 and have continued regularly since 1984 in the expropriated area coded BHD, covering approximately 4000 m^2 (about 1 acre), located east of the Murad II Bath (Fig. S1). Within this area, architectural remains from the Roman and Byzantine periods [2], as well as tile workshops active during the Ottoman era, have been uncovered. To date, eleven kilns dating from the 14th to 17th centuries have been excavated and placed under protection. These kilns produced some of the finest examples of Iznik tiles and ceramics. In accordance with stylistic differences, ceramic artifacts have been classified in the literature under names such as Haliç (Golden Horn) ware, Rodos (Rhodes) ware, Milet (Miletus) ware, and others. Among the excavation findings are kiln wastes—which indicate production and are of great importance for Iznik—as well as semi-finished pieces that were left incomplete due to firing defects, and overfired fragments.

Beyond archaeological and art-historical evaluations of the kiln site, scientific analyses have played a crucial role in revealing production technologies and distinguishing materials originating from different periods and workshops. The first physical and chemical characterization of Iznik ceramics was carried out in the 1950s by Kiefer, head of the laboratory of the National Sèvres Factory, using materials from the

* Corresponding author at: Yildiz Technical University, Department of Metallurgical and Materials Engineering, Davutpasa Campus, 34220 Esenler Istanbul, Türkiye
E-mail addresses: beldemar@istanbul.edu.tr (V.B. Demirsar Arli), gulsu.simsek@yildiz.edu.tr (G. Simsek-Franci).

https://doi.org/10.1016/j.microc.2026.117905
Received 9 February 2026; Received in revised form 27 March 2026; Accepted 30 March 2026
Available online 1 April 2026
0026-265X/© 2026 Elsevier B.V. All rights are reserved, including those for text and data mining, AI training, and similar technologies.

Islamic Arts Department of the Louvre Museum [3–5]. These pioneering studies relied primarily on destructive analytical methods.

Following the initiation of excavations in Iznik in 1963, the number of scientific investigations conducted internationally increased, particularly through the work of foreign researchers. In 1989, Henderson [6,7] employed scanning electron microscopy coupled with energy-dispersive spectroscopy (SEM–EDS) to obtain cross-sectional images and elemental compositions of tile sherds. In the same year, Tite [8] published a study on Iznik pottery, examining Golden Horn, Damascus, polychrome underglaze-decorated, and coral-red wares from the British Museum collection, and determining the chemical composition of pigments used in red, blue, and turquoise decorations.

In Turkey, the first archaeometric research on ceramic finds from the Iznik Tile Kilns Excavation began in the 1990s. Okyar [9] analyzed 22 ceramic samples (nine red-bodied and thirteen white-bodied) using petrographic and microscopic techniques, complemented by elemental analyses of the body, glaze, slip, and decorative layers. Prior to analysis, the samples were sectioned using a precision saw, cold-mounted in epoxy resin, and polished for micro-structure examination with a stereo microscope. Thin sections were also prepared for petrographic observation.

Other researchers who conducted destructive analyses on samples from different periods recovered during the Iznik Tile Kilns Excavations include Kapur et al. [10], Tulun et al. [11], and Kırmızı [12]. In addition, several studies [13,14] have focused on Iznik-type ceramics discovered at other archaeological sites. Although certain analytical techniques employed in these studies (e.g., Raman spectroscopy) are inherently non-destructive, the overall procedures are considered destructive because the samples were cut into cross-sections and, in some cases, embedded in epoxy resin.

In contrast to destructive laboratory-based methods, since the 2018 excavation season, finds have been examined in situ using non-destructive techniques such as digital/stereo microscopy and pXRF [15,16]. Based on chemical compositions obtained from pXRF analyses, select samples were brought to the laboratory for Raman measurements without any sample preparation to identify the phases present in the bodies, the pigments in colored areas, and the molecular structure of the glazes. In situ analyses using non-destructive techniques allow a much larger number of samples to be examined, making statistical studies feasible. Whereas previously only 5–10 samples could be analyzed in the laboratory, more than 50 samples can now be examined within a few hours directly at the excavation site. The short analysis time offered by portable instruments has provided a significant advantage for such technology and provenance studies.

Excavations conducted after the 2010s in the northwestern part of the site, corresponding to the kiln area (Fig. S1b), revealed hundreds of experimental sherds bearing transparent glazes with polychrome brush-applied decorations (blue, turquoise, green, red, and black) of variable thickness and orientation. The assemblage comprises single-sided (tile) and double-sided (ceramic) test samples in flat and sloped shapes, some of which exhibit complete or fractured perforations at the upper margin. In a sense, Iznik potters appear to have carried out their own form of technological experimentation and material testing during this period. In Turkish art-historical discourse, such fragments are commonly referred to as “savor” (çeşni); however, they are designated here as test materials. Based on their white bodies, these sherds were provisionally attributed to 16th–17th century production prior to analysis. Similar test materials were also unearthed during the Tekfur Palace excavations carried out between 1993 and 2001 [17]; however, their number is very limited compared to those recovered from the Iznik Tile Kilns excavations. Moreover, the examples from Tekfur Palace occur exclusively in tile form. Comparable examples from this period have not been identified in Anatolian excavations—apart from those from Iznik and Tekfur Palace—nor in other international archaeological contexts. The first color palettes produced through a comparable approach of technological experimentation in Europe were introduced only in the 19th century by the Sèvres Factory (Manufacture nationale de Sèvres). One of these palettes was produced with colored glazes applied on bisque (fired at 1050 °C), while the other consisted of moufle-fired (880 °C) painting colors displaying different hues of the primary and intermediate colors (>20 colors) [18,19].

In the overall study, approximately 50–60 tile- and ceramic-type samples were examined using digital microscopy, Raman spectroscopy, and portable X-ray fluorescence (pXRF). Nearly half of the samples exhibit severely deteriorated surfaces. Moreover, since the present study aims primarily to focus on ceramic production, only 20 samples with slightly deteriorated or well-preserved surfaces are presented here. The mathematical models used for statistical analyses will be applied in a subsequent study to both tile-type test pieces and to the finished products that are thought to have been produced during the same period.

2. Material and methods

2.1. Ceramic-type study materials

In this study, 20 ceramic-type sherds, glazed and brush-painted in different colors on both sides, were examined (see Fig. 1). While the glaze of some of these samples is well preserved, deterioration of the glaze was observed in others. The transverse dimensions of the samples range from 1 cm to 5 cm. For the small-sized samples (C38, C51, and C61), the chemical composition was determined with a handheld X-ray fluorescence (XRF) spectrometer on only one surface. In some of these samples, perforations can be observed, even if fractured. The perforation may have been used to hold the study material vertically in the kiln to check that the viscosity was not too high, which could have led to sticking. The hole also served to observe whether the glaze wets the surface properly and does not retract. The thickness of the fragments ranges from 4 to 10 mm. In some ceramics, the thickness varies considerably due to curved sections.

2.2. Analytical methods

Prior to characterization, the cross-sections of the sherds were mechanically polished using abrasive papers with grit sizes ranging from 300 to 2000 to remove surface contamination and irregularities.

2.2.1. Digital microscope

After polishing, cross-sectional images of the samples were obtained using a ZEISS Smartzoom 5 digital microscope with a maximum magnification of 335×. These images clearly reveal the glaze, paint, slip, and body layers. Using the microscope's dedicated software (Smartzoom GUI), the thicknesses of the glaze, slip, and painted color layers were measured and listed in Table 1.

2.2.2. Portable handheld X-ray fluorescence (pXRF)

Elemental, semi-quantitative analyses were performed non-destructively using a pXRF spectrometer (Hitachi X-MET 8000 Expert Geo, Oxford Instruments, Abingdon, UK). The instrument was placed in direct contact with the sherds—on the surface for glaze and colored-area measurements, and on the polished cross-section for body analysis. The instrument is equipped with a rhodium (Rh) target X-ray tube (4 W, 50 kV max) and a silicon drift detector (SDD). Measurements were performed using the Mining Light Elements method, which involves two shots: a low-energy shot (10 keV) for the detection of low-Z elements (e.g., Mg and higher) mainly in the ceramic body, and a high-energy shot (40 keV) to identify network modifiers in the glaze and coloring agents in the paints. The beam size at the sample surface was 10.7 mm × 9.4 mm, and a built-in camera was used to monitor the analyzed area. Due to variations in the mineral composition of the body and differences in glaze thickness, measurements were taken at three different locations on the ceramic paste, glaze, and colored areas, with an acquisition time of 30 s per spot. This acquisition time was not arbitrarily chosen but was

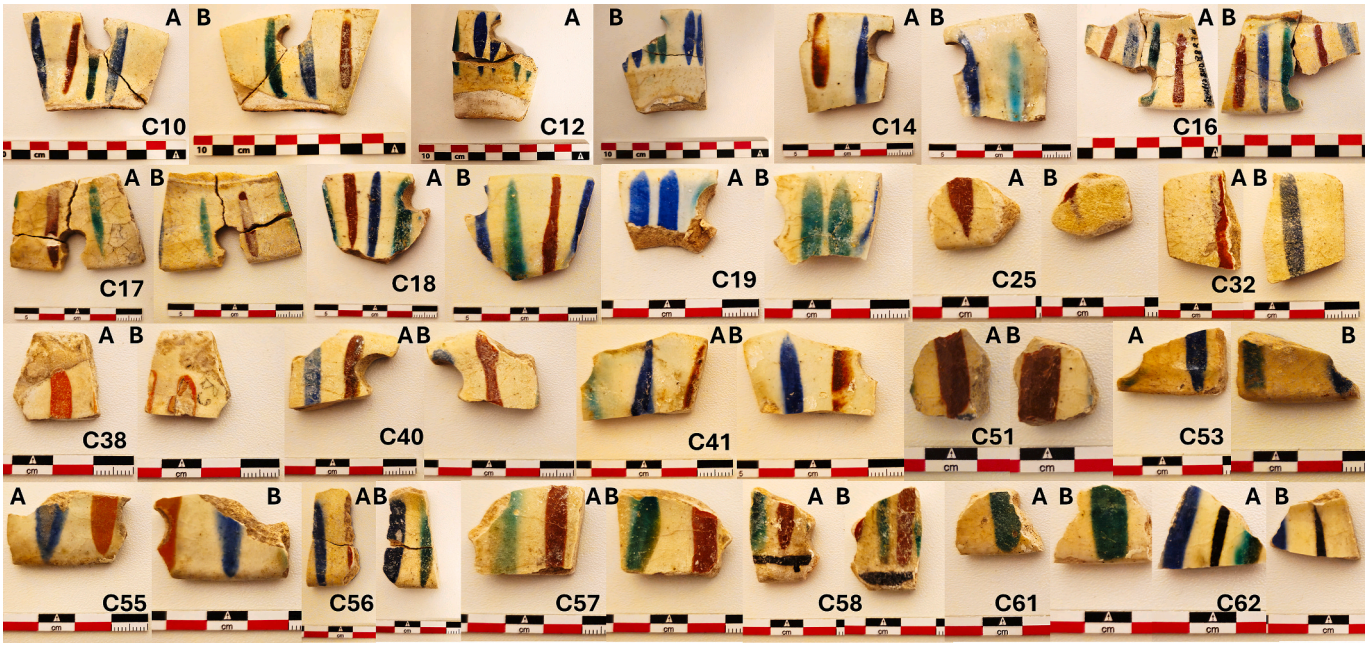


Fig. 1. General view of the ceramic study materials showing the recto and verso surfaces.

Table 1
Description of sherds glazed on both sides. (Re: Red, Blue: Bu, Turquoise: Tu, Green: Gr, Black: Ba, Yellow: Ye, Av: Average, n.m.: not measured).

Code	Colors used in the decor	Color of the paste	Color of the slip	Av. Glaze Thickness (μm)	Av. Slip Thickness (μm)	Sherd Thickness (mm)	Size of free quartz grains in the body (μm)
C10	Bu, Re, Gr	Beige	White	348	442	5.8	~300
C12	Bu, Gr	Whitish	Whitish	308	272	7.0–10.1	<200
C14	Re, Bu, Tu	Whitish	Whitish	150	288	6.0	<200
C16	Re, Gr, Bu	Beige	White	219	315	6.9	~450
C17	Re, Bu, Tu	Beige	Whitish	238	163	5.7	<200
C18	Re, Bu, Gr, Tu	Beige	White	143	265	6.4	<200
C19	Bu, Gr	Dark beige	White	321	367	7.2	>300
C25	Re	Dark beige	White	155	542	5.8	~500
C32	Re, Bu	Beige	White	310	499	6.2	~200
C38	Re	Whitish	Whitish	102	523	4.2	<200
C40	Bu, Re	Beige	White	239	378	7.2	<200
C41	Bu, Re, Tu	Whitish	Whitish	281	313	6.2	<200
C51	Re, Gr	Beige	White	172	422	6.0	~300
C53	Bu, Gr	Beige	White	261	229	6.1	~300
C55	Bu, Re	Beige	White	135	833	5.2–8.6	~400
C56	Bu, Re, Gr	Beige	No slip	421	No slip	5.6–7.3	<200
C57	Gr, Re	Beige	Beige	151	495	7.2	<200
C58	Gr, Re, Ba	Dark beige	White	200	559	7.0	~500
C61	Gr	Beige	White	181	439	6.2	~400
C62	Bu, Ba, Gr	Beige	White	310	327	5.1	~400

Measurement values are given as the average of measurements taken from three different regions.

standardized following a comparison with long-duration WD-XRF analysis [20].

For semi-quantitative evaluation, the Kα lines of major elements (Mg, Al, Si, K, Ca), transition metals (Ti, V, Cr, Mn, Fe, Co, Ni, Cu, Zn, As), and trace elements (Rb, Sr, Zr, Ba, Bi), as well as the L lines of Pb and Sn, were considered. Instrument calibration was verified using mineral standards to ensure accurate measurements and high detection capability of ceramic materials. The standard deviations for the most representative elements—Al, Si, K, Ca, Pb, and Sn—were less than 0.01, whereas Mg, the lowest-Z element measurable by pXRF, exhibited a higher standard deviation of ±0.2. For the comparison with previous results obtained on similar ceramic materials, elemental data was converted to oxides using their appropriate stoichiometric conversion factors.

2.2.3. Confocal Raman spectroscopy

A completely automated Renishaw inVia confocal Raman microscope was used with a 532 nm (green) laser excitation which has a power of 112.5 mW. Systematic Raman measurements were performed using 20× and 50× objectives at laser output powers of 5% (<1 mW), 10% (1–2 mW), and 50% (5–6 mW). The measurement time for each spectrum was 20 s. The spectral range was recorded from 87 to 1339 cm^{-1} for all colors excluding red paint, as well as for transparent glazes. For red pigments, in order to observe the two-magnon scattering peak of hematite at 1320 cm^{-1}, the spectral center was shifted to 785 cm^{-1}, allowing the spectrum to be recorded up to 1371 cm^{-1}. When measurements were attempted in “extended” mode using the Renishaw software (WIRE version 4.4), the Raman spectra became saturated; therefore, all measurements were acquired in “static” mode. The numerical aperture (NA) of the 20× objective is 0.40, while that of the 50× objective is 0.75. The optical sectioning depth depends on the thickness

of the glaze and slip, and measurements at 50% laser power were particularly prone to saturation. No degradation was observed in the decorations of transparent-glazed samples at 5%, 10%, or 50% laser power. In contrast, measurements taken from areas where the glaze was damaged and the red pigment exposed showed phase transformation at 50% laser power. Therefore, Raman spectra obtained at 50% laser power are reported for all measurements except those on red pigments. The baseline of the Raman spectra was performed with the software LabSpec 5 (HORIBA FRANCE SAS).

2.2.4. Data evaluation

For the interpretation and discussion of the results, ternary and binary scattering plots representing the XRF data were generated using Statistica 14.1.0.8 (TIBCO Software Inc., Palo Alto, CA, USA). For the clustering and similarity analysis (dendrogram), the dataset was first explored with the Pandas library. Agglomerative Clustering from the sklearn.cluster module was then applied.

To visualize and interpret the composition of each cluster, dendrograms were generated to display the points within each cluster and their relative distances. Ward's method was selected as the linkage criterion and implemented using the scipy.cluster.hierarchy module for the hierarchical structure and Matplotlib for plotting. All code was developed and executed in a JupyterLab environment (version 4.1.6).

3. Results and discussion

3.1. Microscopic examination

Microscopic observation of the cross sections showed that the glaze thicknesses vary between 421 μm (C56) and 102 μm (C38). Eight sherds contain a glaze layer thinner than 200 μm. Microscopic examination of the blue- and green-decorated area of sample C56 revealed a thick glaze layer, while no slip layer was present. The slip thicknesses of the samples range between 833 μm (C55) and 163 μm (C17). Although sample C55 has a relatively thick slip layer, its glaze layer is thin, measuring 135 μm. In contrast, sample C17 exhibits both a thin slip layer and a glaze layer that is not particularly thick (238 μm). In a comprehensive study on Iznik tiles [21], average glaze thicknesses were reported to be approximately 750 μm, while slip thicknesses ranged from 600 μm to 3 mm. Based on these observations, it is possible to state that tiles and ceramics produced in Iznik workshops display variability in slip and glazing technologies in terms of layer thickness.

When the body thickness of the samples is considered, variations were observed in samples C12, C55, and C56. Sample C12 has a minimum thickness of 7 mm and a maximum thickness of 10 mm; sample C55 ranges from 5 mm to 9 mm; and sample C56 ranges from 5.5 mm to 7 mm. The thicknesses of the remaining samples were examined through repeated measurements and were found to vary between 4 mm and 7 mm. In the study conducted on tiles [22], the thickness of Iznik-produced tiles was reported to range between 11 mm and 18 mm. The differing usage conditions of tiles and ceramics result in variations in their thickness.

In the present study, visual examination indicates that the body colors of the samples vary between white and dark beige tones. The slip layers of some samples are clay-rich and beige in color, whereas others are quartz-rich and white. It is clearly observed that beige-colored bodies have a distinct white slip layer, while whitish or light-colored bodies exhibit a darker, beige slip layer. Moreover, beneath the red decorations, which are mostly embossed, a very clear white slip layer is observed. Differences were also observed in the body microstructures: in some samples, the sizes of free quartz grains are coarse (approximately 500 μm on average), while in others they are finer (< 200 μm). The results of the microscopic examination of the cross sections are summarized in Table 1, and some examples of the cross-section images are shown in Fig. 2.

3.2. Body analysis

Fig. 3 shows the distribution of the contents of Al_2O_3 versus SiO_2 and CaO versus K_2O (wt%) which are presented in Table 2. Based on the pXRF measurements, almost all samples exhibit similar proportions of quartz (73–80 wt%) and alumina (3.5–6 wt%) which confirm the use of stonepaste recipe. Only sample C51 shown in Fig. 4 has a little bit less quartz (68 wt%) and higher amount of alumina (~10 wt%) referring to a clayey body. A previous study [15] conducted on sherds from the Iznik tile kilns identified three groups of body compositions: (i) Group 1,

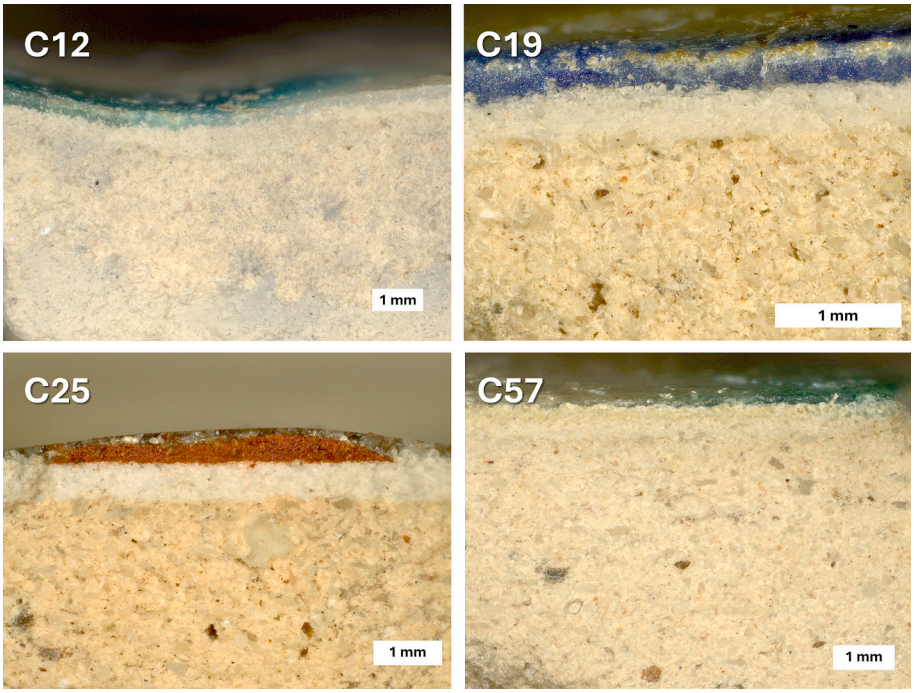


Fig. 2. Representative cross-sections showing different types of body and slip layers observed with the digital microscope.

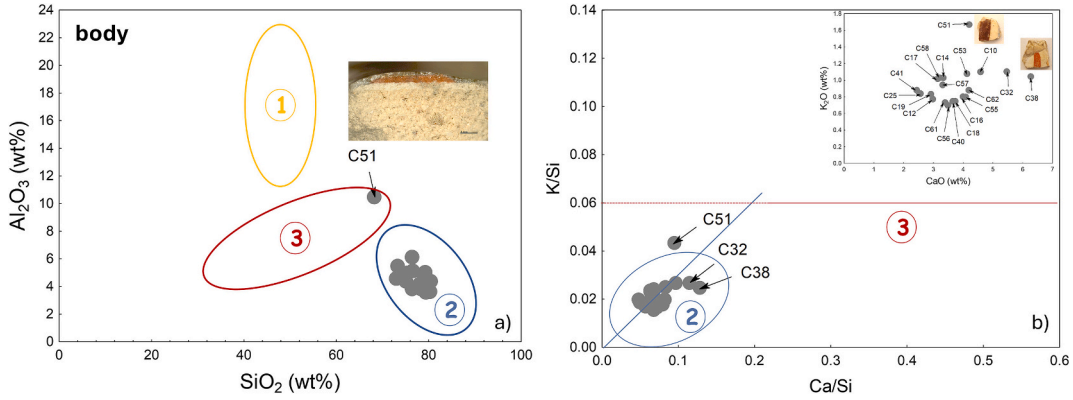


Fig. 3. (a) Binary scatter plots of Al_2O_3 versus SiO_2 (wt%) and (b) K/Si versus Ca/Si showing the previously identified body groups [15] and an enlarged view based on K_2O versus CaO highlighting their compositional distribution in the bodies of the samples (grey circle).

Table 2
Mean values of representative body elements measured by pXRF and converted to their corresponding oxides using conversion factors (wt%).

Code	SiO_2	Al_2O_3	CaO	MgO	Fe_2O_3	K_2O	PbO
C10	73.01	4.54	4.58	3.45	1.39	1.09	5.02
C12	80.38	3.59	2.97	2.74	1.11	0.76	1.65
C14	75.38	4.93	3.33	3.10	0.85	1.02	4.43
C16	79.14	3.73	3.99	1.79	1.25	0.79	2.32
C17	76.42	3.79	3.14	3.02	1.05	1.01	4.10
C18	79.48	3.55	3.73	2.04	0.97	0.74	2.71
C19	79.60	3.88	2.91	2.92	1.05	0.82	1.97
C25	79.30	5.01	2.56	2.57	1.11	0.83	1.78
C32	73.28	5.45	5.47	3.00	1.17	1.10	3.24
C38	75.17	4.35	6.27	2.85	0.98	1.04	2.07
C40	80.46	4.36	3.65	2.13	0.97	0.74	0.82
C41	78.35	3.80	2.44	2.20	0.86	0.87	4.91
C51	68.24	10.46	4.20	3.30	1.97	1.66	1.72
C53	76.43	6.10	4.12	2.50	1.22	1.07	1.38
C55	78.96	4.62	4.08	2.73	0.98	0.79	0.84
C56	79.27	4.13	3.48	2.25	1.03	0.69	2.22
C57	76.54	5.10	3.31	2.92	1.11	0.94	2.79
C58	78.05	4.14	3.20	1.45	1.00	1.02	3.59
C61	79.20	4.08	3.39	1.74	0.84	0.72	3.23
C62	78.08	3.83	4.19	2.72	0.91	0.87	2.50

corresponding to earlier Iznik productions (14th–15th centuries), characterized by higher alumina content and lower quartz content; (ii) Group 2, characterized by low alumina and high quartz content; and (iii) Group 3, characterized by low alumina and low quartz content. In the present study, sample C51 falls into Group 3, whereas the remaining sherds belong to Group 2.

It was also observed that the potassium content in the body of the same sample is higher than in the other samples (~1.7 wt%). The CaO content, on the other hand, is at an average level similar to C53 and C62. In samples C32 and C38, CaO exceeds 5 wt%. Additionally, PbO content in the body of the samples varies between 0.8 and 5 wt% (see Supplementary Material Fig. S2).

The hierarchical clustering method—widely used in archaeometric studies due to its visual interpretability, even for researchers in the social sciences—is one of the most common statistical tools in this field [23,24]. In this study, the hierarchical clustering diagram (Fig. S3), constructed using Ward's method, illustrates changes in total within-cluster variance and confirms the separation of C51 from the main group. This distinction was established by comparing the relationships among samples based on the concentrations (wt%) of minor (MgO, Al_2O_3, K_2O, CaO, PbO, Fe_2O_3), and trace oxides (P_2O_5, Rb_2O, ZrO_2, SrO). SiO_2 was excluded as a major oxide, as its concentration does not vary significantly in these stonepaste-bodied samples.

Raman spectra recorded from the cross-sections of the samples

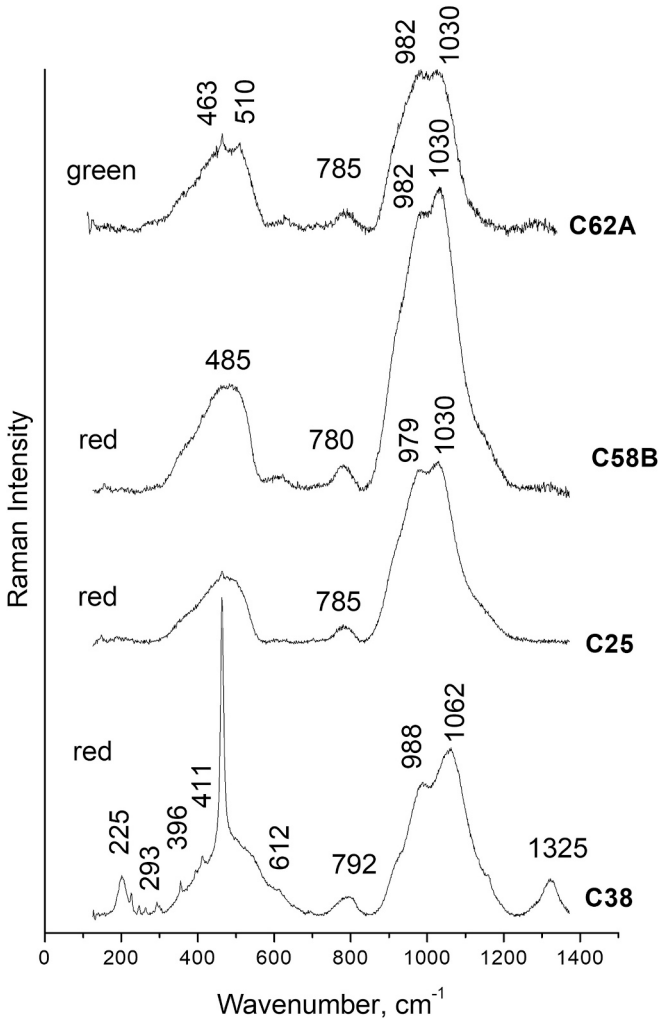


Fig. 4. Representative Raman spectra of samples with low-lead glaze (C38) and lead–alkali glazes.

revealed mainly the presence of quartz (SiO_2), anatase (TiO_2), hematite (Fe_2O_3), calcite ($CaCO_3$), and albite ($NaAlSi_3O_8$) in the body. Due to the structural porosity of the samples, Raman spectra revealed SiC contamination, which was introduced from the abrasive grinding paper during the polishing stage. Based on the chemical composition analyses, only quartz, anatase, and hematite were identified in the ceramic body of sample C51, which is separated from the main group. In addition to

these minerals, spinel was rarely detected in the bodies of samples C10 and C16, while magnetite was identified in the bodies of samples C19 and C40. Spinel and magnetite form under reducing atmospheres and at higher temperatures [25]. In addition, diopside was detected in the body of sample C32 based on the Raman spectra. The presence of diopside indicates a higher firing temperature, exceeding 900 °C. At such temperatures, magnetite remains stable, even above 1000 °C. However, the presence of hematite in sample C32 suggests an oxidizing firing atmosphere. Samples C19 and C40 containing magnetite do not exhibit any hematite phase. Representative Raman spectra are shown in Fig. S4 and the phases found in the samples' bodies are listed in Table 3.

3.3. Glaze analysis

Previous studies [21,26,27] have reported that traditional Iznik ceramic glazes contain between 20 and 40 wt% lead oxide. In the present study, all examined samples except C38 fall within this range, with PbO contents varying between 22 and 40 wt%. In contrast, the glaze of sample C38 contains a significantly lower PbO content of approximately 11 wt%. Interestingly, this sample also contains 0.13 wt% As_2O_3 in the glaze. The chemical composition data of the glazes are provided in the Supplementary Material.

Tin oxide (cassiterite), traditionally used as an opacifying agent, represents an important criterion for distinguishing different production periods of Iznik workshops [8,28,29]. Fig. S5a (see Supplementary Material) shows the distribution of tin oxide versus lead oxide measured in the transparent glaze or in glazes covering a white decorative layer. In the analyzed samples, SnO_2 was detected only at trace levels (0.04–0.67 wt%), indicating that it was present as an impurity rather than as an intentional addition to the glaze recipe. Previous studies on Iznik tiles [21,30] have reported that although the stonepaste body recipe remained largely unchanged until the late 17th century, tin oxide was absent from the glazes of these productions. A later investigation [15] also demonstrated that some 16th- and 17th-century tiles contain only trace amounts of tin (0.2–0.5 wt% SnO_2) and display a relatively wide range of lead contents (22–45 wt% PbO), which is consistent with the results obtained in this study. These observations suggest that the analyzed sherds, decorated with various colors and covered by transparent glazes, most likely correspond to Iznik productions of the later phases of the tradition, possibly dating to the 17th century. In this context, the experimental character of the samples may indicate that the primary objective was to observe color variations as a function of glaze composition rather than to produce opaque glazes using tin-based opacifiers. Alternatively, the craftsmen may not have had consistent access to opacifying raw materials, implying that tin-containing glazes were produced only in specific workshops.

The scatter plot of K_2O versus CaO contents in the glazes (Fig. S5b) reveals mainly two types of fluxes, consistent with previous observations in the literature [6]: one dominated by calcium and another containing both potassium and calcium. The detection of different CaO contents on both surfaces of sample C56 indicates that Iznik ceramicists experimented with modifications in the glaze recipe to obtain different hues in the decorative colors. Similarly, the divergence in CaO–K_2O contents between C17A and C17B suggests the use of different flux compositions on the two surfaces of the same sherd. Samples C61 and C51 are also separated from the main group and cluster together with C56B, suggesting a related glaze formulation.

Similar to tin, the detection of bismuth by pXRF can provide valuable insights into raw material sources and technological practices. Bismuth has previously been reported in the transparent glazes of certain Ottoman tiles [26,31]. Examination of the bismuth oxide–to–lead oxide ratio (Fig. S5c) reveals three groups of glazes: bismuth-free glazes (C14B and C25B), bismuth-independent lead-alkali glazes (30–35 wt% PbO and 0.02–0.06 wt% Bi_2O_3), and bismuth-dependent glazes (C38, C61, and C57A&B). Among these, C57 contains the highest bismuth oxide concentration (0.10 wt%).

Because pXRF measurements performed on the surface of glazed ceramics are sensitive to stratigraphic effects, the thickness of the glaze layer may influence the detected elemental composition. When the glaze is thin, the fluorescence signal can include a contribution from the underlying ceramic body. According to the information depth estimates provided in a previous study [16], reliable determination of lead in a surface layer generally requires a thickness of approximately 300–400 μm, whereas lighter elements may be detected within only a few tens of micrometers. For heavier elements such as tin and barium, the effective information depth may reach several millimeters when commonly used analytical lines are considered. To evaluate whether the measured Pb and Sn values are influenced by glaze thickness, the PbO/SnO_2 ratio obtained by pXRF was plotted as a function of the measured glaze thickness (Fig. S5d). The resulting distribution does not show a systematic relationship between thickness and PbO/SnO_2 ratio. Glazes with similar thicknesses display markedly different PbO/SnO_2 values, suggesting that the observed variations primarily reflect real compositional differences between glazes rather than analytical artifacts caused by thickness effects. Nevertheless, for the thinnest glazes the potential contribution of the ceramic body cannot be entirely excluded and should

Table 3
List of phases found in experimental materials' bodies with Raman.

Sample	Quartz	Anatase	Hematite	Calcite	SiC	Albite	Magnetite	Spinel	Diopside
C10	X			X				X	
C12	X		X	X		X			
C14	X	X							
C16	X			X				X	
C17	X	X	X			X			
C18	X								
C19	X	X		X			X		
C25	X	X							
C32	X	X	X	X			X		X
C38	X				X				
C40	X				X		X		
C41	X	X	X		X				
C51	X	X	X						
C53	X	X							
C55	X	X							
C56	X	X	X						
C57	X		X	X	X				
C58	X	X	X	X	X	X			
C61	X	X			X				
C62	X				X				
Total	20	12	8	7	7	3	3	2	1

be considered when interpreting the pXRF data.

Examination of the Raman spectra of the glazes revealed that, in some samples (e.g., C62A in Fig. 4), a doublet with comparable intensities was observed in the stretching region. However, because sample C38 has the thinnest glaze layer (102 μm), intense quartz peaks originating from the slip are visible in its Raman spectrum, whereas in the other spectra shown in Fig. 4, the quartz peak is weak or absent. The maximum bending band of C58B is located at around 485 cm^{-1}, while in C62A a feldspar-related peak is observed at 510 cm^{-1}.

Sample C38 contains 11 wt% PbO (low-lead glaze). The maximum Si–O stretching band in this sample is located at 1062 cm^{-1}, whereas in samples containing 20–40 wt% PbO the maximum stretching band appears around 1030 cm^{-1}. The higher wavenumber of the stretching band in C38 confirms the presence of an alkali-rich lead-alkali glaze [21,30]. Raman spectra similar to that of C38 have also been observed in some tiles stored in the storage rooms of the Topkapı Palace Museum [21,30]. Among these, samples containing tin oxide were attributed to Iznik production, whereas those lacking tin oxide and characterized by a higher clay content relative to quartz in the body were attributed to Kütahya production [21]. Similar Raman spectra have also been reported in the glazes of Safavid ceramics [32].

Safavid ceramics were produced under the influence of Chinese and Timurid artistic traditions. While these influences are particularly evident in early Safavid ceramics of the 16th century, a distinct Safavid style had become established by the 17th century [33,34]. Ottoman ceramics were also subject to periodic interactions, including the migration of craftsmen to Anatolia (e.g., the issue of Tabrizi masters) and commercial relations, which led to stylistic changes over time. In addition, encounters between the Ottoman court and Chinese porcelain contributed to this process of interaction [33,34]. Overall, it may be suggested that Safavid ceramics were more strongly influenced by Chinese traditions than Ottoman ceramics, while the Ottomans appear to have adopted a more mediated approach, possibly due to local ceramic traditions and historical context [33,34].

3.4. Color analysis

3.4.1. Blue color

In Ottoman tile production, cobalt ores were predominantly used to obtain blue coloration, whereas the use of lapis lazuli appears to have been rare; investigations on this issue are still ongoing. The identification of characteristic impurities present in cobalt ores provides valuable information for determining pigment provenance and, in cases where the origin of the examined object is unknown, may allow inferences to be made regarding its geographical source. Numerous studies have reported the presence of nickel and zinc as impurities associated with cobalt [35], as well as significant amounts of arsenic [36–45].

Analyses of ores collected from several ancient Iranian mining sites have shown that these cobalt ores commonly contain arsenic-bearing phases, suggesting that arsenic-rich cobalt sources may have been historically exploited [46–48]. Moreover, compositional analyses of Ottoman Iznik wares and related productions indicate that cobalt pigments were frequently accompanied by manganese, iron, copper, zinc, and nickel, together with trace (ppm-level) amounts of bismuth, silver, and chromium [15,26,49,50]. Such elemental associations are often interpreted in relation to the geological environment of cobalt deposits: for example, manganese is typically linked to primary mineral deposits, whereas arsenic and bismuth are more characteristic of hydrothermal vein systems. Nickel, in contrast, may occur in both geological settings [51,52].

In the literature [53–55], several types of cobalt sources have been identified depending on the century and the location of mining deposits: (i) the Co–Zn–Pb–In type, newly characterized by elevated Hg content; (ii) the Co–Ni type, containing a considerable amount of Mn; and (iii) the Co–As–Ni–Bi type. The systematically high arsenic (As) content in smalt—sometimes even exceeding the amount of Co—indicates the exclusive use of primary cobalt ores rather than smelting slags. Consequently, the dating of such materials may be shifted to a period after 1573, which corresponds to the documented beginning of targeted cobalt ore mining in the Ore Mountains. By the end of the 17th century, a further increase in arsenic content is observed, likely resulting from the deliberate addition of arsenic oxide as a fining agent.

Visual examination shows that in some samples, the blue decorations appear in dark or light tones with a smooth and vivid appearance (e.g., C19A, C62A, C14A, C18B). In contrast, in certain samples deterioration of the glaze on the surface is observed, which causes the colors to appear dull (e.g., C10A-B, C40A-B, C55A, C56B, C16A). Some of the groups identified through visual examination are also observed in the ternary scatter plots shown in Fig. S6.The distribution of $CoO–As_2O_3–Bi_2O_3$ mainly reveals three groups: one with comparable amounts of arsenic and bismuth, a second group containing bismuth but no arsenic, and a third group (C53B) lacking both arsenic and bismuth. The samples with deteriorated surfaces and dull blue colors (C16A, C55A, C56B) cluster close to each other; they contain lower amounts of cobalt and include certain amounts of arsenic and bismuth. In some samples, such as C55 and C56, it appears that different cobalt sources were used for the blue decoration on the two surfaces. The $NiO–ZnO–As_2O_3$ diagram, on the other hand, indicates one group following the NiO–ZnO trend and another group characterized by arsenic-rich or arsenic-poor compositions within the As_2O_3–NiO–ZnO system. In the samples with dull surfaces (C16A, C55A, and C56B), the amounts of zinc and nickel in the blue pigments are also significantly lower relative to arsenic. For example, sample C10A consists of two fragments that were joined together at a later stage. Among the blue decorations on the A surface, one appears deteriorated, while the other shows no visible signs of alteration. The deteriorated area contains a higher amount of arsenic compared to the non-deteriorated part. However, according to the diagrams presented in Fig. S6, it can be inferred that the same raw material was used in different proportions. The C53B sample, whose cobalt blue contains neither arsenic nor bismuth, is characterized by relatively higher zinc and manganese and lower nickel contents. C32B contains a blue pigment characterized by high amounts of manganese, zinc, and bismuth, but lacking arsenic and nickel; therefore, it stands apart from the other samples. Visual examination indicates not only surface deterioration but also that the blue color appears closer to a blackish tone. In this sample, the color may have resulted from a mixture of pigments rather than a single pigment source.

The analyses indicate that extensive experimentation was carried out by ceramic artisans particularly with the blue pigment, the most characteristic color of Iznik ware. Even within the same sample, different raw materials appear to have been used.

3.4.2. Other colors: green and turquoise hues, red, and black

Fig. S7 illustrates the compositional distribution of the green, turquoise, red, and black colored areas based on the ternary scattering diagrams of $Fe_2O_3–Cr_2O_3–CuO$ and $MnO–Cr_2O_3–MgO$, enabling a more precise identification of the pigments. In general, the $Fe_2O_3–Cr_2O_3–CuO$ scattering diagram shows that the three colors are distinctly grouped. Moreover, within each color group, several compositional subgroups can be distinguished depending on their chemical composition.

Based on the analysis of the black-colored areas, it is understood that two different types of pigments were used, namely spinel and/or chromite. In the black decoration on side B of sample C62, chromium and manganese oxides were detected, whereas a mixture of spinel and chromite was identified on side A. Sample C58 also exhibits black coloration on both sides; however, unlike C62, the same black pigment was used on both surfaces. pXRF measurements revealed relatively high contents of magnesium (1.71 wt% MgO) and iron (0.95 wt% Fe_2O_3), indicating the use of an iron-based spinel pigment.

In the analysis of the green-colored areas, sample C10B was found to contain pigments rich in both copper and chromium. In samples C53A, C57A, and C58B, the copper content is lower while the iron content is

higher. Similar to C10B, sample C58B also contains chromium in addition to copper. In the red-colored areas, manganese (C14A, C14B, C18B, and C55A) as well as chromium (C16A) were detected alongside iron. In some samples, red coloration was measured together with the glaze, whereas in other measurements were taken directly from the red pigment layer. While magnesium oxide was detected in the red pigment of sample C17B in addition to iron, sample C58B exhibits a relatively high manganese oxide content. These observations suggest that different red pigments were employed depending on the workshop, the painter (*nakkaş*), or the production period.

3.4.3. Raman spectra of blue-colored areas

Lead-based glazes generally exhibit rather constant elemental compositions, as they were intentionally used to obtain homogeneous blue areas and are characterized by low viscosity, which promotes effective mixing. As a result, minor and trace elements associated with cobalt are present in low concentrations and may be difficult to detect, especially when the analyzed volume is partly mixed with the ceramic body or a colorless glaze. In addition, the effective probing depth of XRF varies from a few micrometers for light elements (e.g., Al, Si, K, Ca) to several millimeters for heavier ones (e.g. Pb, Sn), depending on both the element considered and the heterogeneity of the décor [16]. While XRF provides information on elemental composition within a given volume, it does not allow phase identification nor discrimination between crystalline and amorphous materials.

Consequently, pigments containing different cobalt-based blue colorants that remain undetected by XRF can often be identified by Raman spectroscopy. Due to the very high coloring power of Co^{2+} ions dispersed in a glassy silicate matrix; an intense blue color can be obtained without reaching the solubility limit or inducing the precipitation

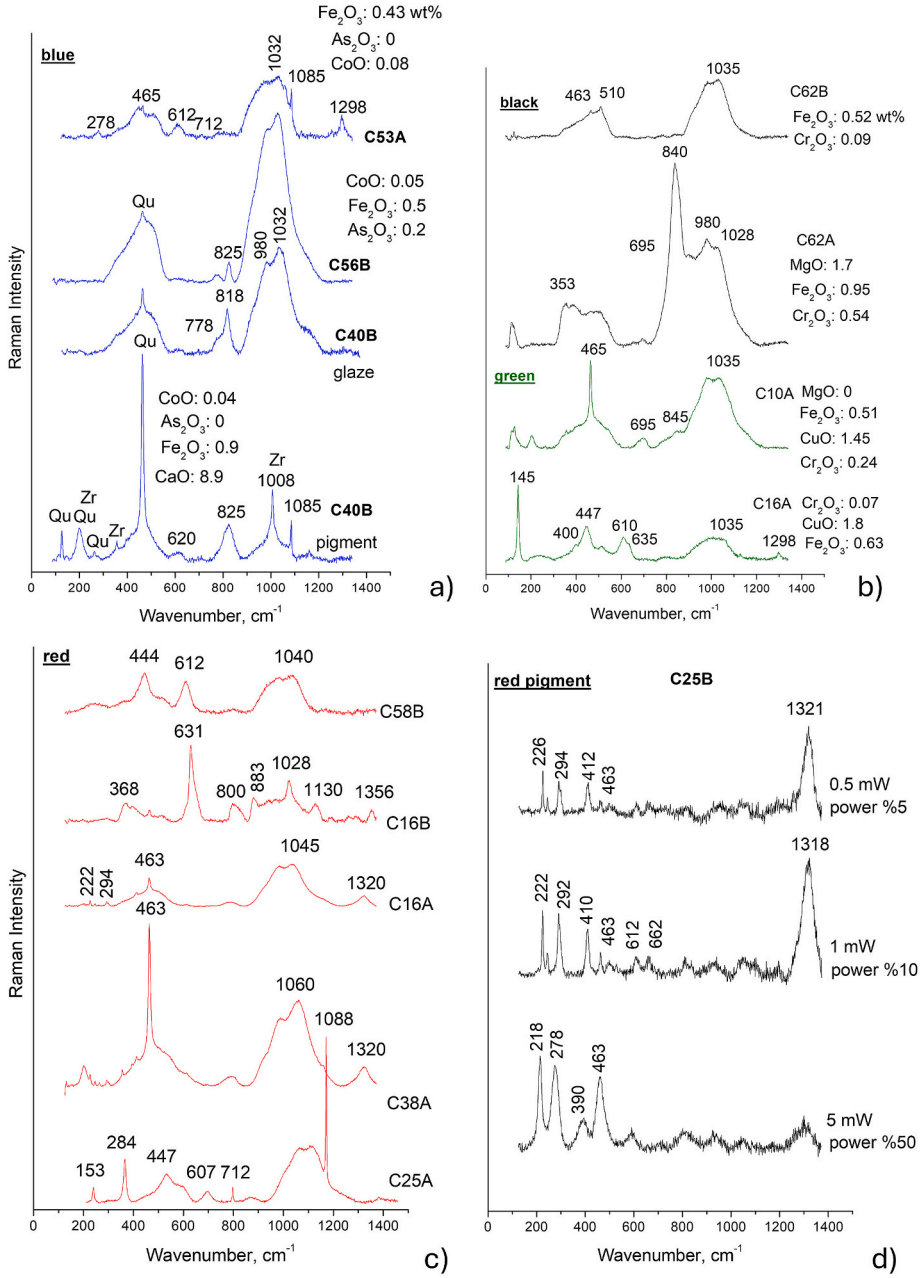


Fig. 5. (a) Raman spectra of blue colored areas, (b) green and black colored areas, (c) red colored areas, and (d) Raman spectra of the same red pigment (C25B) recorded at different laser powers (5%, 10%, and 50%) with 20× objective, showing spectral changes and degradation of red pigment (right). (For interpretation of the references to color in this figure legend, the reader is referred to the web version of this article.)

of crystalline cobalt-bearing phases [48]. Raman spectroscopy is therefore particularly well suited to identifying cobalt-based colorants in such homogeneous glassy systems, even when cobalt-related trace elements are present at very low levels.

The use of arsenic-rich cobalt ores may lead to the precipitation of lead arsenate phases, which are characterized by a strong Raman band at approximately 820–830 cm^{-1}, as reported for objects from the same period [21,30,43,44,52,56,57]. These phases result from reactions between the lead-based glass and As-rich cobalt ores, producing compounds with variable compositions, such as apatite ($Na_{1-x-2y}K_xCa_yPb_4(AsO_4)_3$) [58,59], F-apatite [59], or feldspar [36,60,61], depending on glass composition and firing temperature. The presence of Pb, Na, K, Ca and/or F is related to the fluxes involved in dissolving arsenic from the cobalt ore, with arsenic saturation leading to phase precipitation. The diversity of phases formed accounts for both the shift and the variable bandwidth of the ca. 820 cm^{-1} Raman band. Although elemental arsenic is often difficult to identify by pXRF due to peak overlap with major elements such as lead, its presence is readily detected by Raman spectroscopy through the As–O vibrational mode [52].

Fig. 5 presents the Raman spectra obtained from the blue-decorated glazed surfaces of samples C53A and C56B. For sample C40B, measurements were carried out both on the glazed surface and directly on the blue pigment in an unglazed area. The position of the maximum stretching band at 1032 cm^{-1} indicates a high lead content (≥40 wt%) in this region [30,62].

Since the cobalt content in samples C56B and C40B is extremely low, the trace amounts of arsenic associated with cobalt-bearing pigments could not be detected by pXRF. In the Raman analysis performed directly on the blue pigment, in addition to a broad band centered at 825 cm^{-1}, peaks corresponding to gypsum, calcite, and quartz were observed. According to previous studies on arsenic-containing opacifiers [63], characteristic doublet peaks of apatite appear at 775 cm^{-1} and 820 cm^{-1}. This doublet is observed in both C56B and C40B samples.

On the other hand, the Raman spectrum acquired directly from the blue pigment shows a broad band at 825 cm^{-1}. The widening of this band, together with the increase in its area, can be interpreted as a crystallinity-related effect. Since crystal growth at low temperatures or during very short firing cycles is not possible, more disordered phases tend to form under such conditions. Therefore, the presence of this band in the spectrum obtained directly from the pigment is associated with the firing process [63].

In the Raman spectrum of the blue decoration from sample C53A, no peaks were observed above 800 cm^{-1}. The band detected at 612 cm^{-1} is related to cobalt. The absence of a distinct pigment signature indicates that the blue color was obtained through the dissolution of Co transition metal ions in the glaze matrix [64].

3.4.4. Raman spectra of black-colored areas

In Ottoman ceramic and tile production, black was primarily used for outlining decorative motifs, with the purpose of preventing the diffusion of cobalt- or copper-based pigments. Studies focusing on black contours have shown that chromite, spinel, or mixtures of these phases were commonly employed [21,30,62].

In the present study, black paint is observed on both sides of sample C62. However, both pXRF and Raman analyses (Fig. 5) confirm that the black pigments used on the two sides are different. On side B, no distinct pigment-related Raman features were detected, while pXRF analysis indicates the presence of 0.09 wt% chromium oxide and 0.52 wt% iron oxide. In contrast, side A exhibits higher concentrations of both chromium oxide (0.54 wt%) and iron oxide (0.95 wt%). The Raman spectrum of side A shows a chromite-related band at ~840 cm^{-1} and a spinel-related band at ~695 cm^{-1}, confirming the use of a chromite–spinel-based black pigment.

3.4.5. Raman spectra of green-colored areas

As in the case of cobalt, copper can dissolve into the glassy matrix, making it difficult to detect copper-related phases by Raman spectroscopy [62]. However, in the green decoration of sample C10A, Raman bands corresponding to spinel at ~695 cm^{-1} and chromite at ~845 cm^{-1} were identified. These observations are supported by the pXRF results.

In sample C16A, anatase-related bands are observed at 145, 400, 447, and 635 cm^{-1}. The presence of a band at ~610 cm^{-1}, together with a feature at ~1298 cm^{-1}, indicates the possible contribution of iron-containing phases.

3.4.6. Raman spectra of red-colored areas

Raman measurements of the red decorations were carried out both on the glazed surface and directly on the red pigment in the unglazed areas. In particular, when analyzing iron-based red pigments, the laser power used during Raman analysis is critical in order to avoid degradation effects. For this reason, systematic measurements were performed at different laser power settings (5%, 10%, and 50%) to monitor band deformation.

As shown in Fig. 5, the hematite-related bands observed at 5% and 10% laser power (222, 292, 410, 612, 662, and 1322 cm^{-1}) become weakened, distorted, and slightly shifted when the laser power is increased to 50%. In contrast, the quartz band at 463 cm^{-1} increases in intensity and becomes broader. No phase transformation, such as the conversion of hematite to magnetite, is observed [65]. Instead, the spectra are characterized by deteriorated hematite peaks accompanied by a broadened quartz band. This behavior is consistent with the use of iron-rich sandy materials, such as Armenian bole, in which quartz occurs together with iron (hydr)oxides. Comparable mineral associations have been reported for the Thiviers sandstone employed by French faience manufacturers in the eighteenth century. In Thiviers sandstone, goethite is present in the raw clay prior to firing [66]. In the present spectra, a new band appears at around 390 cm^{-1} as a result of laser-induced degradation, which may be related to the reference Raman band of goethite.

To prevent phase transformations or spectral degradation, Raman measurements on red, hematite-containing ceramic pigments should be conducted at laser powers of 1 mW or lower, as higher powers can weaken, distort, or shift hematite-related bands.

Various types of organic materials are commonly used for the conservation and reassembly of fragmented ceramic objects recovered from archaeological excavations. In the Raman spectrum of sample C16 (Fig. 5), peaks attributed to the adhesive used for joining the fragments were observed (Fig. 5, C16B) [67]. In contrast, no adhesive-related signals were detected on the A side of the same sample; instead, the spectrum is characterized by hematite (222, 294, 1320 cm^{-1}) and quartz (463 cm^{-1}) peaks together with the glaze features in the bending and stretching regions. For sample C58B, only rutile (444, 612 cm^{-1}) a lead–alkali (maximum stretching band at 1040 cm^{-1}) glaze spectrum was identified. Hematite peaks (two magnon scattering of hematite at 1320 cm^{-1}) were detected in sample C38A, while rutile (447, 607 cm^{-1}) and calcite peaks (153, 284, 712, 1088 cm^{-1}) were observed in sample C25A.

3.4.7. Comparison with Tekfur tiles via trace elements content: Iznik or not?

According to information obtained from Ottoman archival sources, a tile workshop was established within Tekfur Palace, located in Edirnekapi, Istanbul, by Nevşehirli Damat İbrahim Pasha. The near cessation of tile production in Iznik created the need for a new tile workshop. In this context, two tile masters were brought from Iznik in 1718 with the aim of producing Iznik-style tiles; however, tiles produced at Tekfur Palace did not reach the level of quality and success achieved by Iznik tiles. Consequently, production came to an end in the 1750s [30].

Excavations carried out at the Tekfur Palace Tile Kilns between 1993

and 1995 and 2000–2001 yielded a wide variety of materials, including glass, ceramic, porcelain, and clay pipe (*lüle*) objects. Among these finds, only a very small number of specimens in tile form, comparable to the study materials recovered from the Iznik Tile Kilns Excavation, were identified [17]. These examples are decorated with linear motifs on only one face and are covered with a transparent glaze. As their reverse sides are undecorated, they are currently displayed fixed to exhibition platforms in the display cases of the Tekfur Palace Museum. Although hundreds of trial pieces have been recovered from Iznik, the fact that such examples have not been found at any other excavated sites in Türkiye and that they have been identified exclusively at Tekfur Palace constitutes significant evidence indicating that Iznik craftsmen either worked at the site or were directly involved in supervising the production.

Considering that craftsmen from Iznik worked at Tekfur Palace, analyses of the glazes and decorative colors were carried out in situ at the museum using portable X-ray fluorescence (pXRF) in order to assess the extent to which production was compatible with Iznik technology and to identify possible different production groups. For two specimens that were found detached from their original context, paste analyses were also performed on cross-sections.

In determining the provenance of a ceramic object, trace elements present as impurities within the body and glaze compositions provide stronger discriminative potential than major elements (Si, Mg, Na, K, Ca in the body; Pb, Na, K, Ca in the glaze) and minor elements (Fe, Ti, Sn, etc.). Zirconium (Zr) originates from quartz, strontium (Sr) from calcium-bearing phases, and rubidium (Rb) from sodium impurities. Chemical compositional analyses indicate that these elements are present at the ppm level. The contents of Zr, Rb, and Sr were therefore used to compare the Tekfur Palace and Iznik groups, and the resulting data were visualized using hierarchical clustering analysis (see Figs. S8 and S9 in the Supplementary Materials). Tekfur Palace samples are designated with the prefix TKF. Based on the trace element concentrations in the glazes, samples TKF03 and TKF04 are separated from the main group and cluster together with sample C38 (characterized by low PbO content), as highlighted in orange in Fig. S8.

As most of the samples were fixed for exhibition purposes, only two unfixed sherds could be examined. Despite the limited number of samples, the results obtained from these two specimens could be compared with those of the C-group samples. Accordingly, as observed in the glaze grouping, TKF 04 (shown in blue) does not fall within any of the defined groups in the body clustering either. In contrast, TKF10 (shown in orange) is compatible with Iznik ceramic bodies.

4. Conclusions

In this study, digital microscopy, pXRF, and Raman spectroscopy were employed for the characterization of 20 ceramic samples decorated and glazed on both sides. These samples represent experimental materials produced by ceramic craftsmen to test colorants and glaze compositions. Archaeometric studies carried out on such materials provide valuable insight into the development of ceramic technology during a specified period.

With the exception of sample C51 (Group 3), all investigated samples were found to have a stonepaste body (Group 2). Variations were observed in slip and glaze thicknesses, and the bodies were shown to contain either coarse or fine free quartz grains. Glaze analyses indicate that none of the samples contain tin oxide, and the interpretation of pXRF data showed that the resulting distribution did not exhibit a systematic relationship between thickness of the glaze and the PbO/SnO_2 ratio. Sample C38 is distinguished from the others by its relatively low lead oxide content in the glaze. Although sample C51 differs in body composition, its glaze composition is consistent with glaze types containing trace or near-trace amounts of tin oxide.

Since ceramics of this type from the Ottoman period have been recovered only from the Tekfur Palace Tile Kilns excavations outside Iznik, the glaze and body compositions of the samples were compared with those assemblages. Some of the productions from Tekfur Palace show complete compositional compatibility with Iznik ceramics, supporting the hypothesis that Iznik-trained craftsmen were active at the Tekfur Palace workshops.

The combined visual observations and elemental distributions suggest the use of multiple cobalt sources in the production of the blue decorations. The ternary diagrams reveal distinct compositional groups, mainly differentiated by the presence or absence of arsenic and bismuth, as well as variations in nickel and zinc contents. Samples with dull and deteriorated surfaces generally cluster together and are characterized by relatively lower cobalt and reduced Ni–Zn contents but measurable arsenic and bismuth. In some cases, different cobalt sources appear to have been used even within the same object or between different surfaces of the same sample. Certain samples display atypical compositions or visual characteristics, indicating either the use of distinct raw materials or the mixing of pigments. Taken together, these observations point to a considerable degree of technological variability and experimentation by ceramic artisans, particularly in the preparation of blue pigments, the most characteristic color of Iznik ceramics, possibly driven by artistic preferences or economic considerations. The analyses of other colors revealed the mixtures of spinel and chromite for black pigments, chromite and spinel together with copper for green decorations, and mixture of hematite and quartz and iron-rich clay materials such as Armenian bole for red pigments. The analytical results demonstrate that XRF and Raman techniques cannot be applied independently in field studies; rather, the two methods are complementary in terms of analytical sensitivity.

CRediT authorship contribution statement

Vesile Belgin Demirsar Arli: Writing – review & editing, Writing – original draft, Resources. **Gulsu Simsek-Franci:** Writing – review & editing, Writing – original draft, Project administration, Methodology, Investigation, Data curation, Conceptualization.

Funding

This work was supported by the Scientific and Technological Research Council of Turkey (TÜBİTAK) through 1001-Scientific and Technological Research Projects Funding Program [grant number 123M874].

Declaration of competing interest

The authors declare that they have no known competing financial interests or personal relationships that could have appeared to influence the work reported in this paper.

Acknowledgements

Tuna Eroğlu and Deniz Eroğlu from TEMS Engineering (Istanbul) is gratefully acknowledged for making Hitachi X-MET 8000 Expert Geo pXRF instrument available in Iznik for on-site measurements. Damla Özeren Şeki (currently at Tetra Teknolojik Sistemler A.Ş.) and Sinan Fidanlıgül from Renishaw Türkiye are also sincerely acknowledged for their invaluable support in the Raman measurements using the Virsa™ Raman analyser.

Appendix A. Supplementary data

Supplementary data to this article can be found online at https://doi.org/10.1016/j.microc.2026.117905.

Data availability

Data will be made available on request.

References

[1] P. Blessing, J.E. Schwartzberg, Maps 5 Anatolia, c.1360-80, in: P. Blessing, R. Goshgarian (Eds.), Architecture and Landscape in Medieval Anatolia, 1100–1500, Edinburg University Press, UK, 2017, p. xviii.

[2] U.M. Ermis, V.B. Demirsar Arli, Appendix to the byzantine churches of Nikaia: newly discovered building at the Iznik tile kilns excavation, ANAR 32 (2025) 254–272, https://doi.org/10.26650/anar.32.1666996.

[3] C. Kiefer, Les céramiques musulmanes d'Anatolie, Cahiers de la Céramique du Verre et des Arts du Feu 4 (1956) 15–30.

[4] C. Kiefer, Les céramiques siliceuses d'Anatolie et du moyen orient, Bulletin de la Société Française de Céramique 30 (1956) 3–24.

[5] C. Kiefer, Les céramiques siliceuses d'Anatolie et du moyen orient, Bulletin de la Société Française de Céramique 31 (1956) 17–34.

[6] J. Henderson, J. Raby, The technology of fifteenth century turkish tiles: an interim statement on the origins of the Iznik industry, World Archaeol. 21 (1) (1989) 115–132, https://doi.org/10.1080/00438243.1989.9980094.

[7] J. Henderson, Iznik ceramics: A technical examination, in: N. Atasoy, J. Raby (Eds.), Iznik: The Pottery of Ottoman Turkey, Alexandria Press, London, 1989, pp. 65–87.

[8] M.S. Tite, Iznik pottery: an investigation of the methods of production, Archaeometry 31 (2) (1989) 115–132, https://doi.org/10.1111/j.1475-4754.1989.tb01008.x.

[9] F. Okyar, Iznik keramiklerinin karakterizasyonu. PhD Thesis, Istanbul Technical University, Graduate School of Science and Engineering, Istanbul, 1995.

[10] S. Kapur, N. Sakarya, E.A. Fitzpatrick, M. Paglial, G. Kelling, E. Akça, C. KaRaman, B. Sakarya, Mineralogy and micromorphology of Iznik ceramics, Anatol. Stud. 48 (1998) 181–189, https://doi.org/10.2307/3643055.

[11] T. Tulun, G. Doner, F. Calisir, N. Cini, N. Karatepe, A. Mericboyu, A. Tekin, A. Altun, B. Arli, H. Arli, An archaeometric study on ancient Iznik ceramics, BAUNFBED 4 (2) (2002) 34–44. https://izlik.org/JA22RW56ZP.

[12] B. Kirmizi, İznik'de bulunan bir grup erken Osmanlı seramiğinde arkeometrik inceleme. M.Sc. Thesis, Middle East Technical University, Graduate School of Science and Engineering, Ankara, 2004.

[13] A. Panagopoulou, D. Lampakis, D. Christophilos, K. Beltsios, T. Ganetsos, Technological examination of Iznik ceramics by SEM-EDX, Raman, XRD, PLM: a case study, Sci. Cult. 4 (3) (2018) 27–33, https://doi.org/10.5281/zenodo.1409802.

[14] J. Burlot, S.Y. Waksman, L. Bellot-Gurlet, G. Simsek Franci, The glaze production technology of an early ottoman pottery (mid-14th (?)-16th century): the case of 'miletus ware', J. Archaeol. Sci. 29 (2020) 102073 https://doi.org/10.1016/j.jasrep.2019.102073.

[15] G. Simsek, B. Demirsar Arli, S. Kaya, P. Colomban, On-site pXRF analysis of body, glaze and colouring agents of the tiles at the excavation site of Iznik kilns, J. Eur. Ceram. 39 (2019) 2199–2209, https://doi.org/10.1016/j.jeurceramsoc.2019.01.050.

[16] B. Demirsar Arli, G. Simsek Franci, S. Kaya, H. Arli, P. Colomban, Portable x-ray fluorescence (p-XRF) uncertainty estimation for glazed ceramic analysis: case of Iznik tiles, Heritage 3 (4) (2020) 1302–1329, https://doi.org/10.3390/heritage3040072.

[17] G. Simsek Franci, Characterization of çeşni tiles from the tekfur palace excavations by portable x-ray fluorescence spectrometry, ITU J. Metal. Mater. Eng. 3 (1) (2026) 20–25, https://doi.org/10.65774/itummej.1845905.

[18] P. Colomban, G. Sagon, X. Faurel, Differentiation of antique ceramics from the Raman spectra of their coloured glazes and paintings, J. Raman Spectrosc. 32 (2001) 351–360, https://doi.org/10.1002/jrs.704.

[19] P. Colomban, M. Gerken, M. Gironda, V. Mesqui, On-site micro-XRF mapping of enameled porcelain paintings and sculpture. First demonstration, J. Eur. Ceram. Soc. 45 (2025) 116849, https://doi.org/10.1016/j.jeurceramsoc.2024.116849.

[20] G. Simsek Franci, Handheld x-ray fluorescence (XRF) versus wavelength dispersive XRF: characterization of chinese blue and white porcelain sherds using handheld and laboratory-type XRF instruments, Appl. Spectrosc. 74 (3) (2020) 314–322.

[21] A.E. Geckinli, G. Simsek Franci, Identification of Tiles in the Storage of Istanbul Topkapı Palace Museum: Final Project Report, Istanbul Technical University Press, Istanbul, 2025.

[22] G. Simsek Franci, V.B. Demirsar Arli, S. Kaya, Color Trials - Establishment of Characterization Methodology of Underglaze Decorated Iznik Tiles with Non-destructive and Portable Spectroscopic Techniques (Raman Spectroscopy and Portable XRF), TÜBİTAK ARDEB Research Program, First Development Report, Ankara, 2025.

[23] L. Maritan, P. Holakooei, C. Mazzoli, Cluster analysis of XRPD data in ancient ceramics: what for? Appl. Clay Sci. 114 (2015) 540–549, https://doi.org/10.1016/j.clay.2015.07.016.

[24] Md.S. Rahman, H.S.C. Metselaar, Abd R. Bushroa, XRF data-based statistical clustering of ancient ceramic artifacts and analysing provenance with thermo-mineralogical analysis, Spectrochim. Acta B At. Spectrosc. 224 (2025) 107090, https://doi.org/10.1016/j.sab.2024.107090.

[25] A. Zopi, E.M. Castellucci, C. Lofrumento, Phase analysis of third millennium Syrian ceramics by micro-Raman spectroscopy, in: H.G.M. Edwards, J.M. Chalmers (Eds.), Raman Spectroscopy in Archaeology and Art History, RSC Analytical Spectroscopy Monographs: Cambridge, UK, 2005, pp. 217–227.

[26] G. Simsek, O. Unsalan, K. Bayraktar, P. Colomban, On-site pXRF analysis of glaze composition and colouring agents of" Iznik" tiles at Edirne mosques (15th and 16th-centuries), Ceram. Int. 45 (1) (2019) 595–605, https://doi.org/10.1016/j.ceramint.2018.09.213.

[27] F. Okyar, The technology of frit making in Iznik, Key Eng. Mater. 264–268 (2004) 2391–2394, https://doi.org/10.4028/www.scientific.net/KEM.264-268.2391.

[28] M. Matin, M. Tite, O. Watson, On the origins of tin-opacified ceramic glazes: new evidence from early islamic Egypt, the levant, Mesopotamia, Iran, and central asia, J. Archaeol. Sci. 97 (2018) 42–66, https://doi.org/10.1016/j.jas.2018.06.011.

[29] R.B. Mason, M.S. Tite, The beginnings of tin-opacification of pottery glazes, Archaeometry 39 (1) (2007) 41–58, https://doi.org/10.1111/j.1475-4754.1997.tb00789.x.

[30] G. Simsek, Characterization of Alkali and Lead-Alkali Glazes with Raman Spectroscopy, PhD Thesis, Istanbul Technical University, Graduate School of Science and Engineering, Istanbul, 2011.

[31] L. Martinet, A. Ben Amara, C. Pacheco, Q. Lemasson, B. Moignard, L. Pichon, P. Colomban, Colored glaze tiles during the ottoman empire (beginning of the 15th to the/ mid 16th century)? EMAC 2015 proc., 13th european meeting on ancient ceramics, 24-26th september 2015, Athens, 2015.

[32] Colomban P., Simsek Franci, G., Timurid, Ottoman, Safavid and Qajar ceramics: Raman and composition classification of the different types of glaze and pigments. Minerals 13(7), 977, https://doi.org/10.3390/min13070977.

[33] N. Atasoy, J. Raby, İznik Seramikleri, TEB & Alexandra Press, London, 1989.

[34] L. Golombek, R.B. Mason, P. Proctor, E. Reilly, Persian Pottery in the First Global age: The Sixteenth and Seventeenth Centuries, Brill, Leiden, 2013.

[35] R. Giannini, I.C. Freestone, A.J. Shortland, European cobalt sources identified in the production of chinese famille rose porcelain, J. Archaeol. Sci. 80 (2017) 27–36, https://doi.org/10.1016/j.jas.2017.01.011.

[36] P. Colomban, B. Kirmizi, C. Gougeon, M. Gironda, C. Cardinal, Pigments and glassy matrix of the 17th–18th century enamelled french watches: a non-invasive on-site Raman and pXRF study, J. Cult. Herit. 44 (2020) 1–14, https://doi.org/10.1016/j.culher.2020.02.001.

[37] B. Gratuze, I. Soulier, J.N. Barrandon, D. Foy, De l'origine du cobalt dans les verres, Revue d'Archéométrie 16 (1992) 97–108, https://doi.org/10.3406/arsci.1992.895.

[38] B. Gratuze, I. Soulier, M. Blet, L. Vallauri, De l'origine du cobalt: Du verre à la céramique, Revue d'Archéométrie 20 (1996) 77–94, https://doi.org/10.3406/arsci.1996.939.

[39] P. Colomban, Y.Z. Zhang, B. Zhao, Non-invasive Raman analyses of chinese huafalang and related porcelain wares. Searching for evidence for innovative pigment technologies, Ceram. Int. 43 (2017) 12079–12088, https://doi.org/10.1016/j.ceramint.2017.06.063.

[40] P. Colomban, F. Ambrosi, A.T. Ngo, T.A. Lu, X.L. Feng, S. Chen, C.L. Choi, Comparative analysis of wucai chinese porcelains using mobile and fixed Raman microspectrometers, Ceram. Int. 43 (2017) 14244–14256, https://doi.org/10.1016/j.ceramint.2017.07.172.

[41] P. Colomban, B. Kirmizi, B. Zhao, J.B. Clais, Y. Yang, V. Droguet, Investigation of the pigments and glassy matrix of painted enamelled qing dynasty chinese porcelains by non-invasive on-site Raman microspectrometry, Heritage 3 (2020) 915–940, https://doi.org/10.3390/heritage3030050.

[42] R.G.V. Hancock, J. McKechnie, S. Aufreiter, K. Karklins, M. Kapches, M. Sempowski, J.-F. Moreau, I. Kenyon, Non-destructive analysis of european cobalt blue glass trade beads, J. Radioanal. Nucl. Chem. 244 (2000) 567–573, https://doi.org/10.1023/A:1006705014455.

[43] F. Koleini, L.C. Prinsloo, W.M. Biemond, P. Colomban, A.T. Ngo, J. Boeyens, M. van der Ryst, K. van Brakel, Unravelling the glass trade bead sequence from magoro hill, South Africa: separating pre-17th-century asian imports from later european counterparts, Herit. Sci. 4 (2016) 43, https://doi.org/10.1186/s40494-016-0113-2.

[44] F. Koleini, P. Colomban, I. Pikirayi, L.C. Prinsloo, Glass beads, markers of ancient trade in sub-Saharan africa: methodology, state of the art and perspectives, Heritage 22 (2019) 343–369, https://doi.org/10.3390/heritage2030144.

[45] J. Molera, A. Climent-Font, G. Garcia, T. Pradell, O. Vallcorba, A. Zucchiatti, A study of historical processing of cobalt arsenides in XV-XVI century europe, J. Archaeol. Sci. Rep. 36 (2021) 102797, https://doi.org/10.1016/j.jasrep.2021.102797.

[46] G. Ladame, Les ressources métallifères de l'Iran, Schweiz. Mineral. Petrogr. Mitt. 25 (1945) 165–298.

[47] M. Matin, A.M. Pollard, From ore to pigment: a description of the minerals and experimental study of cobalt ore processing from the kāshān mine, Iran, Archaeometry 59 (2017) 731–746.

[48] M. Matin, A.M. Pollard, Historical accounts of cobalt ore processing from the kāshān mine, Iran, Iran 53 (2015) 171–183.

[49] M.S. Gill, T. Rehren, Material characterization of ceramic tile mosaic from two 17th century islamic monuments in northern India, Archaeometry 53 (2011) 22–36, https://doi.org/10.1111/j.1475-4754.2010.00537.x.

[50] B. Constantinescu, D. Cristea-Stan, I. Kovacs, Z. Szokefalvi-Nagy, External milli-beam PIXE analysis of the mineral pigments of glazed Iznik (Turkey) ceramics, Period. Mineral. 83 (2014) 159–169, https://doi.org/10.2451/2014PM0009.

[51] Kissin, S.A., 1992. Five element (Ni-Co-As-Ag-Bi) veins. Geosci. Can. 19, 113–124. Available online: https://journals.lib.unb.ca/index.php/gc/article/view/3768/4282/ (accessed on 14 March 2026).

[52] P. Colomban, B. Kırmızı, G. Simsek Franci, Cobalt and associated impurities in blue (and green) glass, glaze and enamel: relationships between raw materials, processing, composition, phases and International Trade, Minerals 11 (2021) 633.

[53] Z. Čermáková, D. Hradil, J. Míková, J. Hradilová, D. Rohanová, Co-glass and blue pigment smalt production at the turn of the 15th/16th centuries: LA-ICP-MS study, Archaeol. Anthropol. Sci. 18 (68) (2026) 1–18, https://doi.org/10.1007/s12520-025-02402-4.
[54] Y. Porter, Le cobalt dans le monde iranien (IXe-XVIe siècles), Taoci 1 (2000) 5–14.
[55] J. Henderson, Blue and other coloured translucent glass decorated with enamels: Possible evidence for trade in cobalt-blue colourants, in: R. Ward (Ed.), Gilded and Enamelled Glass from the Middle East, BMP, London, UK, 1998, pp. 116–121.
[56] P. Colomban, L. Arberet, B. Kırmızı, On-site Raman analysis of 17th and 18th century Limoges enamels: implications on the european cobalt sources and the technological relationship between Limoges and chinese enamels, Ceram. Int. 43 (2017) 10158–10165, https://doi.org/10.1016/j.ceramint.2017.05.040.
[57] P. Colomban, B. Kirmizi, Non-invasive on-site Raman study of polychrome and white enamelled glass artefacts in imitation of porcelain assigned to Bernard perrot and his followers, J. Raman Spectrosc. 51 (2020) 133–146, https://doi.org/10.1002/jrs.5745.
[58] B. Manoun, M. Azdouz, M. Azrour, R. Essehli, S. Benmokhtar, L. El Ammari, A. Ezzahi, A. Ider, P. Lazor, Synthesis, rietveld refinements and Raman spectroscopic studies of tricationic lacunar apatites Na1-xKxPb4(AsO4)3 (0 < x < 1), J. Mol. Struct. 986 (2011) 1–9, https://doi.org/10.1016/j.molstruc.2010.09.043.
[59] P. Colomban, M. Maggetti, A. d'Albis, Non-invasive Raman identification of crystalline and glassy phases in a 1781 Sèvres royal factory soft paste porcelain, J. Eur. Ceram. Soc. 38 (2018) 5228–5233, https://doi.org/10.1016/j.jeurceramsoc.2018.07.001.
[60] A. Kremenovic, P. Colomban, B. Piriou, D. Massiot, P. Florian, Structural and spectroscopic characterization of the quenched hexacelsian, J. Phys. Chem. Solids 64 (2003) 2253–2268, https://doi.org/10.1016/S0022-3697(03)00252-X.
[61] J.J. Freeman, A. Wang, K.E. Kuebler, B.L. Jolliff, L.A. Haskin, Characterization of natural feldspars by Raman spectroscopy for future planetary exploration, Can. Mineral. 46 (2008), https://doi.org/10.3749/canmin.46.6.00, 1477-100.
[62] G. Simsek, A.E. Geckinli, An assessment study of tiles from topkapı palace museum with energy- dispersive x-ray and Raman spectrometers, J. Raman Spectrosc. 43 (2012) 917–927, https://doi.org/10.1002/jrs.3108.
[63] J. Burlot, D. Vangu, L. Bellot-Gurlet, P. Colomban, Raman identification of pigments and opacifiers: interest and limitation of multivariate analysis by comparison with solid state spectroscopical approach—II. Arsenic-based opacifiers and relation with cobalt ores, J. Raman Spectrosc. 55 (2024) 184–199, https://doi.org/10.1002/jrs.6612.
[64] Tournié, A., Prinsloo, L.C., Colomban P., 2010. Raman spectra database of the glass beads excavated on Mapungubwe hill and k2, two archaeological sites in South Africa. https://hal.Science/hal-00543867v1 retrieved on 05.02.2026.
[65] D.L.A. De Faria, S. Venancio Silva, M.T. de Oliveira, Raman microspectroscopy of some iron oxides and oxyhydroxides, J. Raman Spectrosc. 28 (11) (1997) 873–878, https://doi.org/10.1002/(SICI)1097-4555(199711)28:11<873::AID-JRS177>3.0.CO;2-B.
[66] A. Sempio, A. Gualtieri, Mineralogy of the grès de thiviers (northern Aquitaine, France), Period. Mineral. 71 (1) (2002) 65–84.
[67] M. Asquier, P. Colomban, V. Milande, Raman and infrared analysis of glues used for pottery conservation treatments, J. Raman Spectrosc. 40 (2009) 1641–1644, https://doi.org/10.1002/jrs.2312.